Journal of the European Ceramic Society 18 (1998) 1365–1371

PII: S0955-2219(98)00066-1
0955-2219/98/$—see front matter

Powder Processing of Mullite/Mo Functionally Graded Materials*

A. P. Tomsia,[a†] E. Saiz,[a] H. Ishibashi,[b] M. Diaz,[c] J. Requena[c] and J. S. Moya[c]

[a]Lawrence Berkeley National Laboratory, Berkeley, CA 94720, USA
[b]TOTO Ltd, Kitakyushu, Japan
[c]Instituto de Ciencia de Materiales de Madrid, CSIC, Cantoblanco, 28049 Madrid, Spain

Abstract

Graded or layered materials have been used for many years in specific applications to improve reliability for bonds between dissimilar materials, for improved coating adherence and to obtain better compatibility between fibers and matrices in composites. Recently, the concept has been formalized, and such materials entitled FGMs. Molybdenum and mullite are two ideal candidates to fabricate ceramic/metal composites and FGMs because of their similarity in thermal expansion, lack of reactivity at high temperature and high refractoriness. In the present work a systematic investigation of powder processing for the fabrication of mullite/Mo FGMs is described. It was found that the processing of mullite/Mo in water resulted in a formation of a homogeneous composite, whereas mixtures processed in ethyl alcohol produced FGMs with continuous gradient. Compositional gradients, fracture toughness, hardness and electrical conductivity of the FGMs were also evaluated. © *1998 Elsevier Science Limited. All rights reserved*

1 Introduction

A functionally graded material (FGM) is one in which composition, microstructure and properties vary continuously across the material. Such materials would be useful in applications where different properties are needed at different surfaces and where reducing the residual and applied stress distributions is critical for functionality and lifetime improvement. Although such structures have been developed heuristically, the desire to develop unified concepts for FGM design is relatively new and has prompted the reformulation of key questions regarding design principles to yield materials with optimal performance and reliability.[1]

Examples where FGM structures could be useful include: (1) the joining of dissimilar materials, e.g. ceramics with superalloys for gas turbines or for turbocharger rotor-to-shaft; (2) bonding electrodes to electrolytes, as for fuel cells; (3) creating structures with thermal barriers, such as high-speed air foils; (4) bonding electrodes to insulating containment, as for high energy lamps and (5) forming environmentally compatible transition layers, as for biomaterials implants.

Mullite/Mo FGMs have several advantages: (i) both compounds exhibit very similar thermal expansion values ($\alpha_{Mo} = 5{\cdot}75\times10^{-6}°C^{-1}$, $\alpha_{Mull} = 5{\cdot}13\times10^{-6}°C^{-1}$, at 1000°C),[2,3] thus, the residual thermal stresses due to thermal expansion mismatch are expected to be very small; (ii) there is a range of temperature and $p(O_2)$ for which mullite and Mo are compatible, which facilitates processing and ensures the chemical stability of the composite under certain operating conditions; (iii) Mo is an good electrical and thermal conductor ($\rho_{Mo} = 5{\cdot}6\times10^{-6}\,\Omega cm$, $\kappa_{Mo} = 138\,W\,m^{-1}\,K^{-1}$ at room temperature)[2] whereas mullite is an electrical insulator and has a very low thermal conductivity ($\kappa_{Mull} = 2{\cdot}5\,W\,m^{-1}\,K^{-1}$).[4] This opens a large number of possible applications in electronics and microelectronics, in thermal barrier coatings or in electrical conductor/insulator components.

Recently Ishibashi *et al.*[5] have developed SiO_2/Mo continuous FGM for electrodes used in high-intensity discharge lamps. The present investigation describes the development of mullite/Mo FGMs using pressure slip casting method.

2 Experimental Procedure

The following starting powders have been used: 99·9% pure Mo metal (Kojyundo Kagaku, Japan)

*Presented at the International Conference 'Powder Characterization for Advanced Materials Manufacture', Gijón, Spain, 16–20 June 1997.

†To whom correspondence should be addressed at Center for Advanced Materials, Lawrence Berkeley National Laboratory, 1 Cyclotron Road, MS 62-203, Berkeley, CA 94720, USA.

with an average particle size of 1·5 μm; Mullite (Chichibu MP40, Scimarec Co. Ltd, Tokyo, Japan) with an average particle size of 0·7 μm and TiO_2, 0·08; MgO, 0·04; CaO, 0·07; Fe_2O_3, 0·05; Na_2O, 0·02 and K_2O, 0·04 wt% as main impurities.

In order to process mullite/Mo FGMs by the pressure slip casting method, slurries containing 50 wt% solids have been prepared using 200 proof ethyl alcohol or distilled water as liquid media. The mixtures were homogenized by milling with alumina balls in polyethylene containers at 120 rpm for 3 h. The slip casting was made in cylindrical PMMA tubes (2 cm diameter) placed on plaster of Paris blocks. The pressure has been kept constant at 0·375 MPa for 2 h. Subsequently, the cylindrical green samples with have been dried at 40°C in air for 48 h. After drying, the specimens were sintered in vacuum (5×10^{-3} Pa) at 1650°C for 1 h. The final FGMs are cylinders with ~15 mm radius and the gradient parallel to the height (typically 10–20 mm).

In parallel, the sedimentation behavior of the different slurries in glass test tubes has been studied at room temperature for times up to 24 h. In the case of water-based mixtures, the liquid was filtrated after the tests and the remaining solid was analysed by micro-Raman spectroscopy (Dilor, Argon+, $\lambda = 514{\cdot}5$ nm).

Sintered FGMs were mounted in an epoxy resin and cut perpendicular to the gradient. The cross-sections were fine ground and finished by polishing with diamond. The final abrasive used was 0·25 μm Al_2O_3. The microstructure of sintered and polished specimens was evaluated using reflected light optical microscopy (Leica DMRM, Germany), scanning electron microscopy (SEM, Topcon, DS-130C) and transmission electron microscopy (JEOL 2010, 200 KeV). The major phases present in the sample were identified by XRD. Elemental analysis and X-ray mapping were performed both by energy dispersive (EDS) and wavelength dispersive (WDS) methods. The phase concentration profile along the FGM normal axis has been obtained by SEM/EDS analysis on the polished cross-section of the sample using Mo $L_{\alpha 1}$ peak intensity quoted from an area of 50×200 μm, with the short dimension parallel to the gradient.

Electrical resistivity measurements have been performed on FGM slices of ~1 mm thick. The slices were cut perpendicular to the gradient. The resistivity was measured using the 4-point method with d.c. currents between 0 and 500 mA, silver paint contacts and pure copper wiring. Mo content in each slice was determined by EDS analysis.

The variation of hardness and toughness along the gradient was measured using Vickers indentation of polished cross-sections. The loads were adjusted in order to obtain indentations having well-defined radial cracks, which could be used to compute the fracture toughness, but without lateral cracking or spalling (small loads give indentations with no cracks and excessive loads cause spalling). This resulted in the use of loads varying from 50 to 100 N, with higher loads being required for the higher Mo contents. From the measured indentation and crack size both the hardness and fracture toughness were calculated. The toughness was calculated from the relation given by Anstis *et al.*[6] as:

$$K_{IC} = 0{\cdot}16\left(\frac{E}{H}\right)^{1/2}\frac{P}{C^{3/2}} \qquad (1)$$

where E is the Young's modulus; H, the hardness; P, the indentation load; and C, the measured crack length. Only the results of tests with long cracks ($C/D > 2$, D indentation diagonal) were used to measure toughness. The elastic moduli were calculated based on the Mo concentration using the rule of mixtures.

3 Results and Discussion

3.1 Sedimentation and processing

The sedimentation studies showed that the water-based slurries flocculate forming mullite/Mo clusters. The coagulated suspension settles very fast, resulting in homogeneous sediment with relatively low packing density. Consequently, all attempts to fabricate graded materials using water-based slurries has been unsuccessful, with the final product being a homogeneous mullite/Mo composite. On the other hand, alcohol-based slurries remained deflocculated, and the mullite and Mo particles settle at different velocities given by their density (10·2 g/cm^3 for Mo and 3·16 g/cm^3 for mullite) and size (Fig. 1). The final sediment has a larger packing density and presents a continuous gradient in Mo content from top to bottom. Therefore it has been possible to obtain mullite/Mo FGMs using the alcohol-based slurries. The final gradient is determined by two processes, on one side the different sedimentation velocity of the metal and ceramic particles, as given by the Stokes law, and on the other, the progressive drying of the slurry that starts from the bottom (the face touching the plaster of Paris). The sedimentation behavior is different in the SiO_2/Mo system, where continuos FGMs can be prepared using water-based slurries.[5]

The pH of the mullite powder suspension in water is 6·1, close to the isoelectric point of mullite, 6·03.[7] The molybdenum powder used in this study was found to contain a small amount of oxide on

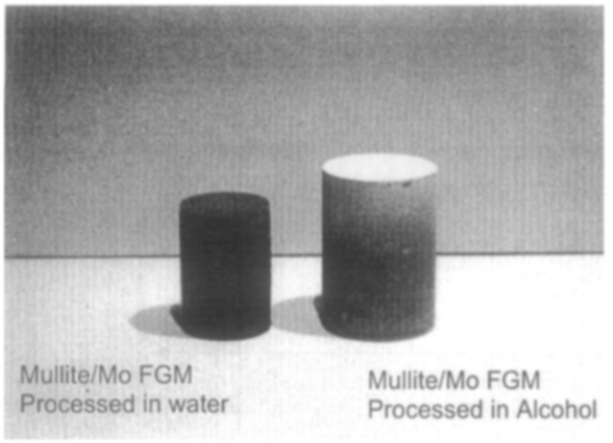

Fig. 1. Mullite/Mo green compacts obtained by pressure slip-casting of ethyl alcohol and water slurries.

its surface (the weight loss of the Mo powder after hydrogen annealing at 600°C for 2 h was 0·56%). When the molybdenum particles are present in water a partial dissolution of the molybdenum oxide layer takes place. The Mo oxide is responsible for the bluish color observed in the supernatant liquid.[8] This dissolution induces the formation of $(Mo_7O_{24})^{6-}$ species[9] and shifts the pH to 4·1. These species are stable in the pH range 3–6·5[9] and can be adsorbed on the surface of the molybdenum particles, as has been observed by micro-Raman spectroscopy of the solid fraction separated from the water slurries (Fig. 2). This spectrum is in good agreement with the one proposed by Coddington and Taylor[9] for $(Mo_7O_{24})^{6-}$. At pH = 4·1 mullite particles are positively charged and consequently will be attracted by the negatively charged molybdenum species present on the surface of the Mo particles. A coagulated, open and loose structure, similar to the one presented in Fig. 3, forms and hinders the differential sedimentation of Mo and mullite grains.

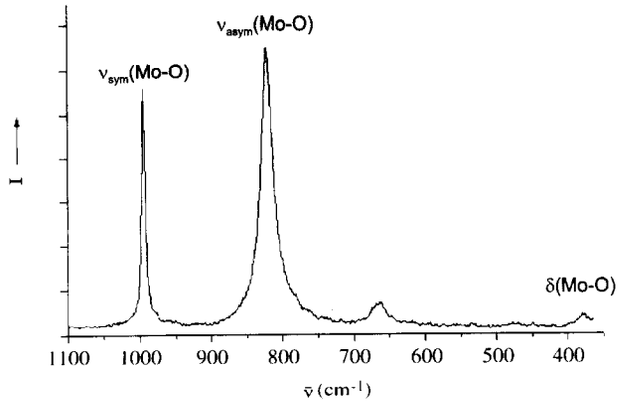

Fig. 2. Raman spectrum obtained from the water slurry solid fraction after drying in air. The characteristic vibrational frequencies ν_{sym}(Mo–O), ν_{asym}(Mo–O) and δ(Mo–O) associated with $[Mo_7O_{24}]^{6-}$ species at 993, 822 and 379 cm^{-1}, respectively, can be seen.

Fig. 3. Schematic representation of the aggregation state of mullite and molybdenum particles in water slurries.

In the silica/Mo system processed in water no flocculation has been observed.[5] In this system Mo particles settle as expected based on the difference in specific gravity between Mo and silica. This makes processing of silica/Mo FGM relatively easy. In this particular case formation of $(Mo_7O_{24})^{6-}$ also takes place shifting the pH toward the acid region of pH 3–4. However, at these pH values the silica particles are negatively charged ($SiO_{2i.e.p.} = 2$[10]), and therefore no attraction forces between negatively charged molybdenum species and silica occurs.

3.2 Microstructural study

The sintered mullite/Mo FGMs had a density >99% th. and a continuous graded microstructure. A typical optical micrograph of the cross-sectioned FGM is shown in Fig. 4. Figure 5 shows the fraction of molybdenum (vol%) versus length fraction. Once the slurry is poured into the mold, a cake forms almost immediately at the bottom surface, giving the observed sharp peak in Mo concentration. This is because the coarser molybdenum particles settle very fast at the beginning of the pressurized slip casting operation. The final shape of the gradient depends on the combination of differential sedimentation of the metal ceramic particles and drying of the slurry. The final gradient shows an increase in Mo content until it reaches a maximum value at about 0·4 length fraction. Then, the Mo content decreases monotonically to almost zero at the top of the sample.

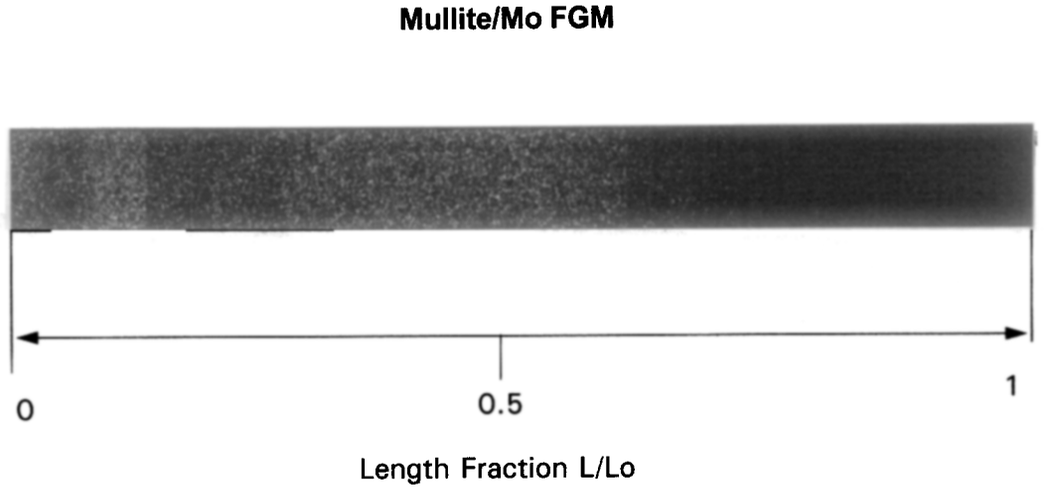

Fig. 4. Reflected light optical micrograph corresponding to a mullite/Mo FGM cross-section showing the molybdenum (white particles) concentration gradient.

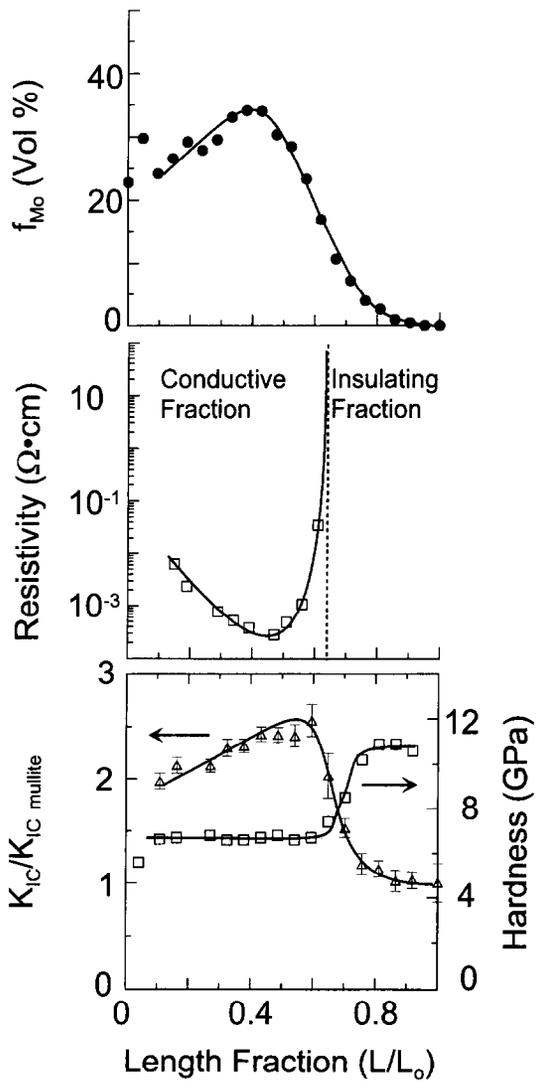

Fig. 5. Plots of fraction of Mo (vol%), resistivity, toughness and Vicker's hardness versus length fraction for mullite/Mo FGM.

Typical SEM micrographs of the FGM obtained at different distances from the bottom (Mo-rich part) are shown in Fig. 6. It is important to note that no new phases were detected by XRD or

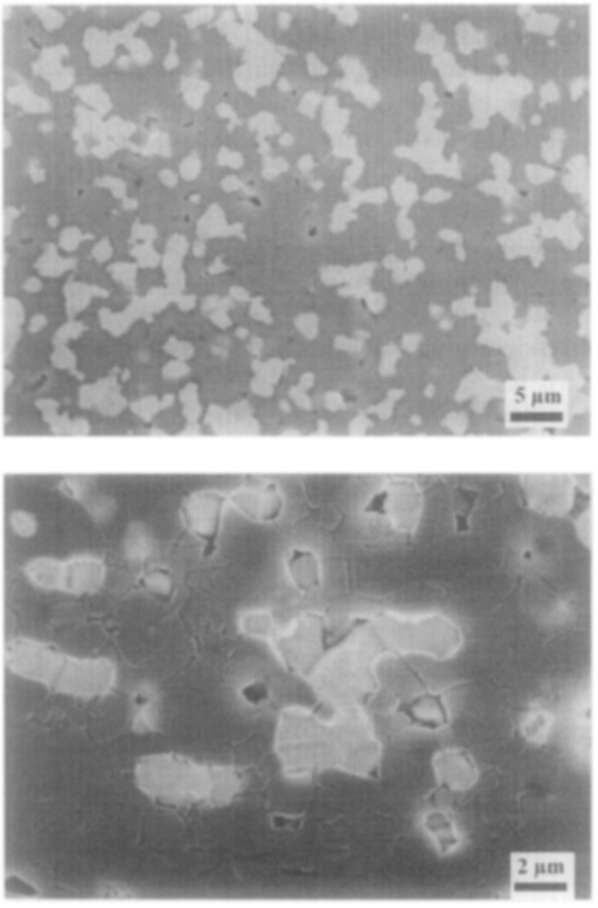

Fig. 6. SEM micrographs of mullite/Mo FGM specimen obtained at different distance from the bottom.

observed at the mullite/Mo interface by TEM or SEM. A TEM micrograph of the interface is shown in Fig. 7. The EDS analysis of the Mo particle shows the presence of oxygen. This oxygen is located at the interstitial position of the bcc lattice of Mo causing embrittlement of the metal.[11] The analysis of mullite exhibits a Mo peak, which corresponds to an amount of 2·3 wt% of Mo dissolved in mullite. This suggests that the Mo oxide that coats the metal particles diffuses into the mullite lattice.

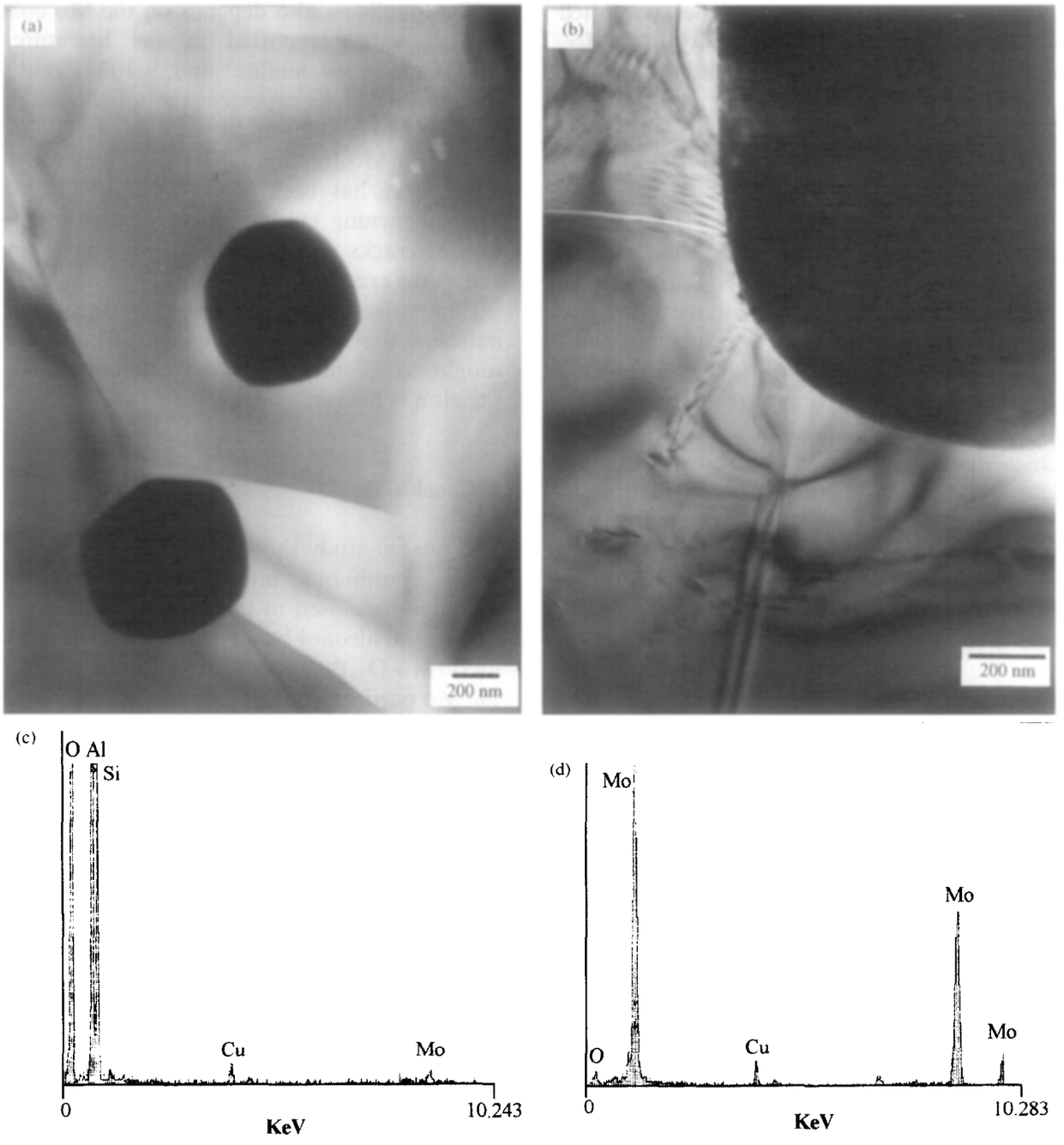

Fig. 7. (a) TEM micrograph showing molybdenum particles inside mullite grains. (b) Close-up of a mullite/Mo interface showing no presence of new phases at the interface. (c) EDS spectrum obtained from a mullite grain indicates about 2·33 wt% of molybdenum. (d) EDS spectrum obtained from a molybdenum particle showing the presence of oxygen.

No data have been reported in literature about the solid solution of Mo oxides in mullite. Extensive synthesis experiments performed by Schneider[12] have shown that mullite can incorporate into its structure different amounts of a wide variety of transition metals, e.g. Ti, V, Cr, Mn, Fe and Co. Schneider *et al.*[13] also studied the thermal expansion of mullite with additions of 11·5 wt% Cr_2O_3 and 10·3 wt% Fe_2O_3 (close to the solubility limit for these oxides in mullite). He concluded that Cr^{3+} and Fe^{3+} are incorporated in mullite by replacement of Al^{3+}. Mo^{3+} has an ionic radius in the same range as Cr^{3+} and Fe^{3+} (0·65 Å) when located in an octahedral coordination. Consequently, Mo^{3+} can also substitute Al^{3+} in the mullite lattice. A more detailed study will be necessary to completely understand the mechanism and the extension of this solid solution.

3.3 Electrical properties

Figure 5 shows the resistivity of each FGM slice depending on its location in the specimen. It can be observed that ~2/3 of the sample conducts electricity. The transition from conductor to insulator marks the point where the microstructure changes from an interconnected metal–ceramic composite to isolated metal particles in a mullite matrix.

In Fig. 8 the resistivity of each slice is plotted against its Mo content. The resistivity of a Mo–ceramic composite can be modeled using the General Effective Media equations[14] as:

$$\rho_c = \rho_{Mo}\left(1 - \frac{1 - f_{Mo}}{1 - f_c}\right)^{-t} \quad (2)$$

where ρ_c is the resistivity of the composite, f_{Mo} the volume fraction of the composite, f_c the critical volume fraction needed for conductivity (for Mo contents lower than f_c the slice is insulating) and t is an exponent that is fitted from the experimental data and depends on the composite microstructure.

Fitting of the resistivity data with the General Effective Media Equation is also shown in Fig. 8. The corresponding critical Mo volume fraction (f_c) is about 12 vol% and $t \sim 3{\cdot}2$. The expected f_c for a random distribution of conductive and non-conductive spheres of same size is 16%,[14] slightly larger than measured. This can be due to the effect of particle size distribution. Possible strategies to decrease the critical fraction of Mo needed for the conductivity (f_c) would include the development of microstructures in which the conductive particles are not packed at random (e.g. have arrays of conductive particles in the form of strings) or to use Mo particles with more elongated shapes (for example, fibers).

3.4 Hardness and toughness

As can be seen in Fig. 5 the hardness varies weakly with Mo content, up to the maximum at the mullite side of the FGM. This dependence is reasonable, given reported values of 15 GPa for mullite[15] and of 2–2·5 GPa for annealed Mo.[2]

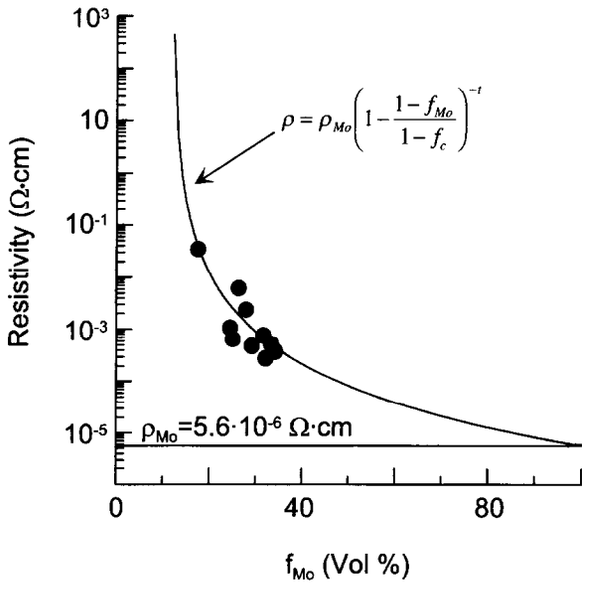

Fig. 8. Electrical resistivity of thin FGM slices depending on their Mo content. Fitting to the General Effective Media equation is also presented.

The toughness also depends on the Mo content. Typical values reported in the literature are 2·0 MPa·m$^{1/2}$ for mullite[3] and 5–10 MPa·m$^{1/2}$ for sintered Mo.[16] As expected, the toughness increases with Mo content up to twice the mullite toughness for a Mo fraction of 35%. Similar toughness dependence has been found in Mo/SiO_2 FGMs. The toughening mechanism involves some deflection of cracks and bridging of metallic ligaments across the crack flanks.

Comparison with the resistivity measurements indicates that the larger change in hardness and toughness occurs when the interconnected Mo skeleton is broken.

4 Conclusions

The present study shows that it is possible to fabricate continuous mullite/molybdenum FGMs, with density closed to theoretical, by pressure slip casting of alcohol-based slurries. When water is used $(Mo_7O_{24})^{6-}$ species adsorb on the surface of the Mo particles causing flocculation and impeding the formation of graded structures.

Mullite and Mo do not react during sintering in vacuum at 1650°C and no new phases were detected in the final FGM. On the other hand, EDS analysis detected the presence of oxygen in the Mo grains and ~2·3 wt% of Mo in the mullite lattice.

The mechanical properties (hardness and toughness) and electrical resistivity varied along the gradient as expected. An important point is that it has been possible to fabricate FGMs with a microstructure that continuously changes from an interconnected metal/ceramic composite to metal particles isolated in a mullite matrix to almost pure ceramic. As a result, the samples contain both a conductive and insulating areas.

Acknowledgements

Work supported by Director, Office of Energy Research of US Department of Energy under Contract No. DE-AC03-76SF00098. Additional funding was also obtained from TOTO Corporation and from NATO Grant CRG Programme SA.5-2-05(CRG970082). This work has been partially supported by CICYT Spain under contract No. MAT97-0724.

References

1. Hirai, T., Functional gradient materials. In *Processing of Ceramics, Part 2*, ed. R. J. Brook, chapter 20, in *Materials Science and Technology Vol. 17B*, ed. R. W. Cahn,

P. Haasen and E. J. Kramer. VCH Verlagsgesellschaft, Weinheim, Germany, 1996.
2. Smithells, C. J. (Ed.), *Metals Reference Book*, 5th edn, Butterworths, London, 1978, pp. 940–943 and 1257.
3. Skoog, A. and Moore, R., Refractory of the past for the future: mullite and its use as a bonding phase. *Am. Ceram. Soc. Bull.*, 1988, **67**(7), 1880–1885.
4. Lackey, W. J., Stinton, D. P., Cerny, G. A., Schaffhauser, A. C. and Fehrenbacher, L. L., Ceramic coatings for advanced heat engines—a review and projection. *Adv. Ceram. Mat.*, 1987, **2**(1), 24–30.
5. Ishibashi, H., Saiz, E. and Tomsia, A. P., Mo/SiO_2 FGMs fabricated by slip casting. *Am. Ceram. Soc. Bull.*, 1997, **76**(4), 231.
6. Anstis, G. R., Chantikul, P., Lawn, B. R. and Marshall, D. B., A critical evaluation of indentation techniques for measuring fracture toughness: I, Direct crack methods. *J. Am. Ceram. Soc.*, 1981, **64**(9), 533.
7. Moreno, R., Moya, J. S. and Requena, J., Rheological parameters of mullite in aqueous suspensions. In *Ceramics Today—Tomorrow's Ceramics*, ed. P. Vicencini, Elsevier Science Publishers B.V., 1991, pp. 1053–1061.
8. Müller, A., Meyer, J., Krickemeyer, E. and Diemann, E., Molybdenum blue: a 200 years old mystery unveiled. *Agnew. Chem. Int. Ed. Engl.*, 1996, **35**, 1206–1208.
9. Coddington, J. M. and Taylor, M. J., Molybdenum-95 nuclear magnetic resonance and vibrational spectroscopy studies of molybdenum (VI) species in aqueous solutions and solvent extracts from hydrochloric and hydrobromic acid: evidence for the complexes $(Mo_2O_5\ (H_2O))^{2+}$, $(MoO_2X_2(H_2O))$ (X = Cl or Br), and $(MoO_2Cl_4)^{2-}$. *J. Chem. Soc. Dalton. Trans.*, 1990, 41–47.
10. Reed J. S., *Introduction to the Principles of Ceramic Processing*. John Wiley and Sons, 1988, p. 134.
11. Kumar, A. and Eyre, B. L., Grain boundary segregation and intergranular fracture in molybdenum. *Proc. R. Soc.*, 1980, **A370**, 431–458.
12. Schneider, H., Transition metal distribution in mullite. *Ceram. Trans.*, 1990, **6**, 135–158.
13. Schneider, H. and Eberhard, E., Thermal expansion of mullite. *J. Am. Ceram. Soc.*, 1990, **73**, 2073–2076.
14. McLachlan, D. S., Blaszkiewicz, M. and Newnham, R., Electrical resistivity of composites. *J. Am. Ceram. Soc.*, 1990, **73**(8), 2187–2203.
15. Schneider, H., Okada, H. K. and Pask, J. A., *Mullite and Mullite Ceramics*. John Wiley and Sons, New York, 1994, pp. 199–205.
16. Archer, R. S., Briggs, J. Z. and Loeb, C. M. Jr, *Molybdenum: Steels, Irons, Alloys*. Climax Molybdenum Company, New York, 1970, p. 5.